Nanoscale

PAPER

View Article Online
View Journal | View Issue

Cite this: *Nanoscale*, 2016, **8**, 13463

Adsorption orientations and immunological recognition of antibodies on graphene†

J. G. Vilhena,[a,b] A. C. Dumitru,[a] Elena T. Herruzo,[a] Jesús I. Mendieta-Moreno,[b,c] Ricardo Garcia,*[a] P. A. Serena[a] and Rubén Pérez*[b,d]

Received 3rd November 2015,
Accepted 7th June 2016

DOI: 10.1039/c5nr07612a

www.rsc.org/nanoscale

Large-scale molecular dynamics (MD) simulations and atomic force microscopy (AFM) in liquid are combined to characterize the adsorption of Immunoglobulin G (IgG) antibodies over a hydrophobic surface modeled with a three-layer graphene slab. We consider explicitly the water solvent, simulating systems with massive sizes (up to 770 000 atoms), for four different adsorption orientations. Protocols based on steered MD to speed up the protein diffusion stage and to enhance the dehydration process are combined with long simulation times (>150 ns) in order to make sure that the final adsorption states correspond to actual stable configurations. Our MD results and the AFM images demonstrate that the IgG antibodies are strongly adsorbed, do not unfold, and retain their secondary and tertiary structures upon deposition. Statistical analysis of the AFM images shows that many of the antibodies adopt vertical orientations, even at very small coverages, which expose at least one Fab binding site for recognition events. Single molecule force spectroscopy experiments demonstrate the immunological response of the deposited antibodies by recognizing its specific antigens. The above properties together with the strong anchoring and preservation of the secondary structure, make graphene an excellent candidate for the development of immunosensors.

The study of protein interaction with material surfaces is a subject of fundamental and technological interest. Proteins constitute the largest and most widely employed class of biomolecules for surface functionalization. There is a wide range of applications in biotechnology that rely on protein adsorption such as biocompatible interfaces, biosensors, and interfaces for tissue engineering and regenerative medicine.[1–7] One common requirement for those applications is that the protein must remain bioactive upon deposition. Protein adsorption also represents an interesting and important fundamental problem because it is the result of the interplay among protein–surface interactions, hydration forces, and the protein ability to change conformation as controlled by its internal strength. Over the past few years, many experimental studies have addressed the challenge of understanding and controlling protein–surface interactions.[1] Nevertheless, due to the inherent difficulties to probe events at an atomistic level, protein adsorption is not well understood yet.[1,7] As a result, the design of most devices dependent on protein–surface interactions is still based on trial and error approaches.[1,7]

Different biomedical applications[2,8] such as immunoassays[9,10] and biosensors[11] would benefit from a better understanding of the Immunoglobulin G (IgG) adsorption upon solid surfaces. IgG is the most abundant among the five classes of antibodies produced by the body and provides the majority of the antibody-based immune response.[12] IgG is a glycoprotein complex composed of four peptide chains arranged in a Y-shape. It is formed by two antigen binding fragments (Fab) and one crystallizable fragment (Fc) (see Fig. S1†). The antigen binding sites (paratopes), located at the far end of the Fabs, are extremely variable, thus allowing the recognition and binding to one specific antigen epitope.[13] This ability to bind to a specific antigen, which characterizes the bioactivity of a given IgG, is extremely sensitive to the conformational structure of the paratope.[1,14] In order to improve the sensitivity of current immunoassays, many experimental methods for controlling the antibody adsorption orientation have been thoroughly investigated. This has proved to be a highly non trivial task since, for all the surfaces studied so

[a]*Instituto de Ciencia de Materiales de Madrid (ICMM), CSIC, c/Sor Juana Ines de la Cruz 3, E-28049 Madrid, Spain. E-mail: r.garcia@csic.es*
[b]*Departamento de Física Teórica de la Materia Condensada, Universidad Autónoma de Madrid, E-28049 Madrid, Spain. E-mail: ruben.perez@uam.es*
[c]*Centro de Biología Molecular Severo Ochoa, CSIC-UAM, E-28049 Madrid, Spain*
[d]*IFIMAC – Condensed Matter Physics Center, Universidad Autónoma de Madrid, E-28049 Madrid, Spain*

† Electronic supplementary information (ESI) available: Further details concerning the experimental methods, the MD simulation protocols, and the characterization and stability of the different adsorption configurations. See DOI: 10.1039/C5NR07612A

far,[14–20] including mica, quartz, silica and pentacene, the IgG seems to preferentially adsorb in *Flat*-on orientations. These orientations make the Fabs less accessible than vertical configurations and, consequently Fabs could lose their biofunctionality. As a result, except in the recent study of 2D crystals built from IgG domains (fragments),[21] the IgG biochemistry is diminished.

Graphene, the leading carbon-based two dimensional material proposed to develop novel electronic devices, would be an ideal substrate for biomedical applications. Graphene has already been considered to develop biosensors, medical implants and drug delivery systems.[22] All of these applications require to address its biocompatibility and biosafety.[23] To assess the suitability of graphene as a support surface for a new generation of biosensors and, in particular, immunosensors, it is crucial to characterize how the antibody adsorbs (its orientation and adsorption energy) and the subsequent effects on its bioactivity. Previous work has shown that, independently of the ionic strength and pH, antibodies show a high affinity for hydrophobic surfaces.[15] Therefore, graphene being hydrophobic, one expects it to be able to immobilize IgGs. While a high adsorption affinity is a required feature to develop IgG-based biosensors, a strong adsorption could lead to an undesired protein unfolding or to a loss of its bioactivity.[24]

An ideal surface for IgG adsorption should prevent any major unfolding of the protein and should also leave the Fabs pointing towards the solution. From an experimental perspective, it is very challenging to determine both the actual adsorption orientation of a given antibody as well as the degree of adsorption-induced unfolding on IgG. The high lateral resolution of force microscopy (AFM) and its ability to image individual molecules on different environments makes AFM an ideal technique for this task. Force microscopy studies of antibody deposition and adsorption have been performed in air and liquid on different surfaces such as mica,[21,25–28] pentacene[20] or biological membranes.[29,30] High resolution images have revealed some of the dominant adsorption configurations but they can only provide very limited information about the different factors that lead to the observed morphologies. Accurate atomistic simulations in the protein native liquid environment are a perfect complement to these experiments in order to gain this fundamental understanding. The overall protein adsorption process is composed of three main stages:[1] diffusion of the protein from the bulk solution into the interface region, dehydration of the protein/surface interface, and, finally, deformation and attachment of the protein onto the surface. Previous combined studies, focused on the adsorption of small peptides,[7,31,32] have validated the use of simulation methods – such as molecular dynamics (MD), steered-molecular-dynamics (SMD), and the associated classical force fields – to gain direct, quantitative information about the competing mechanisms involved in the adsorption of small protein fragments. These calculations use an accurate atomistic description of the solvent, including explicitly the water molecules in the simulations. Extending this approach to large proteins like the IgG, with more than 20 000 atoms and a molecular weight of 150 kDa, is a very challenging task, due to the sheer size of the calculations (involving $\sim 10^6$ atoms) and the long simulation times needed to describe the diffusion and dehydration stages.[33] Previous theoretical studies of protein adsorption on graphene or alike hydrophobic surface graphene where water is considered explicitly have been restricted to short peptide-chains[31,34,35] or small proteins like BMP-2 (26 kDa).[36] Larger proteins like BSA (66 kDa) have been addressed[37–42] using an implicit solvent approach. All of these studies have demonstrated an almost complete loss of the secondary structure, suggesting that the IgG would unfold and lose its bioactivity once it is adsorbed upon graphene. However, this evidence has to be considered with caution. Sun *et al.*[43] have found differences in the adsorption behavior with the solvent model used. Furthermore, earlier results for the unfolding of moderately large proteins like lysozyme (14.3 kDa, 125 amino acids) coming from implicit solvent studies[40] have been questioned by more recent simulations using explicit water models.[33,44] From a more fundamental perspective, it is not clear if the free energy balance, that results in the unfolding of the small peptides on hydrophobic surfaces, holds in the case of an entire protein that presents strong internal binding interactions.

Here we combine large-scale molecular dynamics (MD) simulations and high resolution atomic force microscopy imaging in liquids to study the adsorption of IgG antibodies on graphene. We have included water explicitly, simulating systems with massive sizes (up to 770 000 atoms) for very long simulation times (>150 ns) in order to make sure that the final adsorption states corresponds to actual stable configurations. Protocols based on steered MD have been devised to speed up the protein diffusion stage, to enhance the dehydration process, and to determine the adsorption energies. Our theoretical and experimental results conclusively demonstrate that the IgG antibodies are strongly adsorbed on graphene, do not unfold upon adsorption, and retain their secondary structure. These results show that the energy balance controlling adsorption on hydrophobic surfaces depends on the size and internal strength of the protein. For large proteins like the IgG, adsorption is dominated by protein–substrate van der Waals interactions, while hydrophobic forces seem to play a very minor role. Furthermore, near half of the antibodies adsorb in vertical orientations that expose both Fab binding sites for the specific binding to antigens. Force spectroscopy measurements demonstrate the immunological response of the deposited antibodies by selectively interacting with their specific antigens. Those features make the IgG/graphene system a candidate for the next generation of biosensors.

Results and discussion

MD simulations for IgG adsorption

We have considered the four different molecular orientations, that have been identified and named in previous studies,[14,15] for the adsorption of antibodies on a surface (see Fig. 1 and

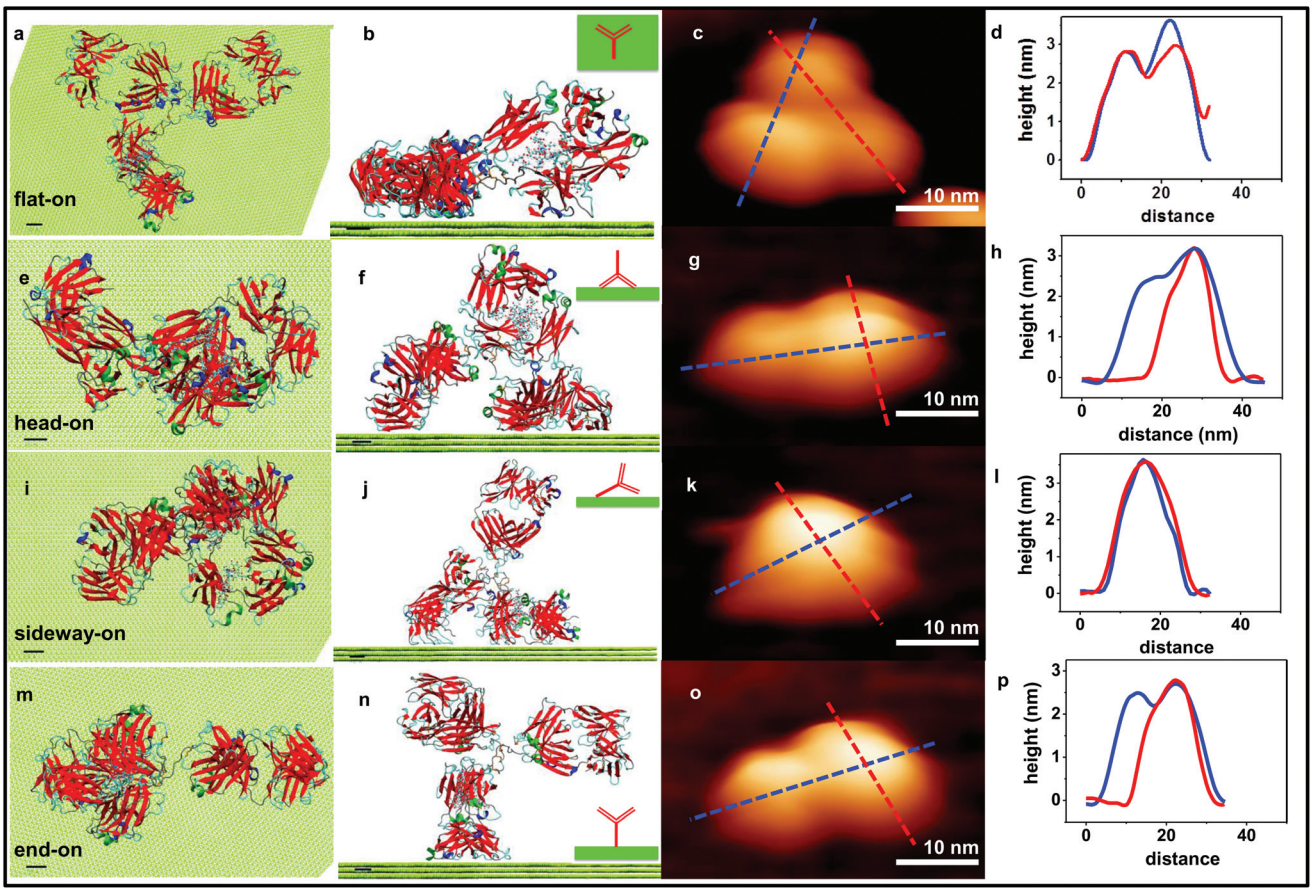

Fig. 1 Stable adsorption configurations of IgG on graphene in water. From left to right, the first two columns correspond to the structures for the four different orientations after 152 ns of MD simulations, while the other two display AM-AFM images that reveal these characteristic adsorption configurations. Panels a, e, i and m (b, f, j, n) show the corresponding top (side) views. The IgG is represented with its secondary structure: beta-sheets (red), alpha-helix (dark-green), 3_{10}-helix (dark-blue), turns (cyan), and random-coils (light-gray). The two glycan chains present on the Fc domain are represented using a ball-and-stick model, while the sulfur-bridges are highlighted in dark-orange. The light green atoms in the theory panels correspond to the carbon atoms in 20 × 20 nm^2 ABA stacked 3-layer graphene slab used as a substrate in the MD simulations. Panels c, g, k and o show the topographic AFM images of the four orientations adopted by the IgG antibodies adsorbed on graphene. Panels d, h, l and p display the corresponding cross-sections along the lines marked in the images. The assignment of each AFM image to a given orientation is further supported by the inter-domain distances measured in Fig. S5,† that are in very good agreement with the ones determined from the final MD structures (see Table 2).

S1†): *Flat*-on (all the three fragments adsorbed to the support), *End*-on (only the Fc adsorbed), *Sideway*-on (one Fab and the Fc adsorbed) and *Head*-on (both Fabs adsorbed). In order to speed up the slowest part of the adsorption process, protein diffusion from the solution into the interface region, we have used SMD to apply a gentle force on the IgG hydrophobic backbone – in particular, 30 S-bonded cysteine alpha carbons (see Methods and Fig. S2† for details), that brings the protein closer to the substrate, intensifying the dehydration while keeping the internal structure intact. Including this enhanced adsorption stage, the whole protocol that we have applied for the simulation of each orientation is as follows: firstly, we position the IgG (PDB ID: 1IGT) in one of the four orientations at a distance of 10 Å from a 20 × 20 nm^2 three-layer graphene slab with A–B–A stacking, and we solvate the system with TIP3P water molecules (150 000–250 000 depending on the orientation).[45] Then, we heat up the system at 300 K, leave the IgG to freely adsorb during 10 ns, apply the enhanced adsorption for 2 ns, and, finally, let the system equilibrate for another 140 ns.

The first two columns of Fig. 1 present the top and side view of the final adsorption configuration for each of the four characteristic orientations of the antibodies after 152 ns of MD simulation. We have used a manifold of different properties, including the total energy and their components, the root-mean-square-deviation of the protein with respect to its initial configuration (RMSD), the gyration radius tensor (RoG), the contact surface area, and the solvent accessible surface area, in order to characterize the adsorption mechanism and to verify that the process has indeed been completed and that a final stable configuration has been reached. The time evolution of all of these quantities provides a very detailed picture of the process. The rapid evolution and final stabilization of the total energy, and of the protein–surface contact area (see Fig. 2) in

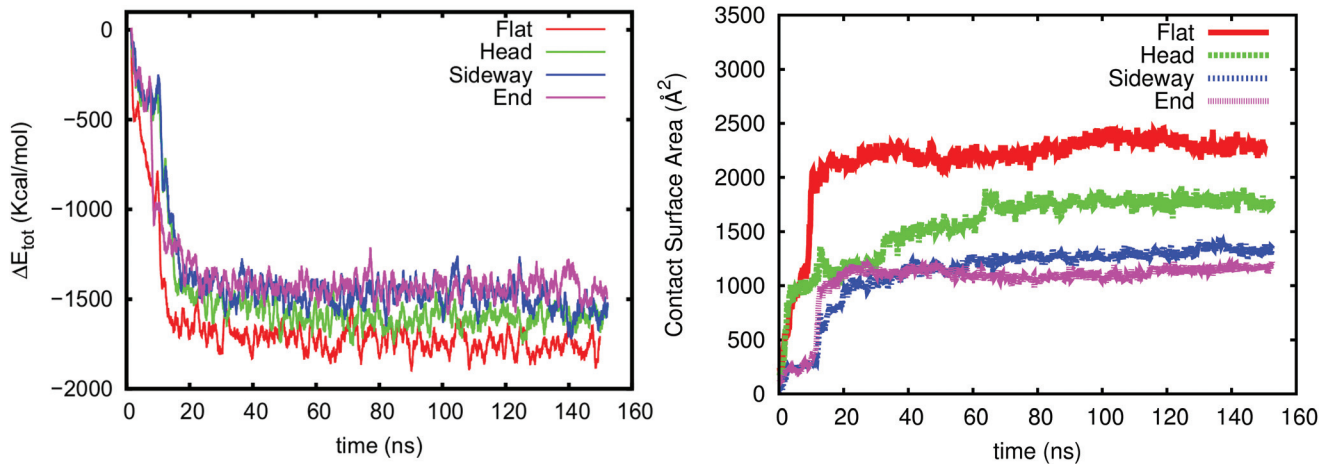

Fig. 2 Evolution of the total energy (left) and the contact area between the protein and surface (right) during the MD simulations (152 ns) for the different adsorption orientations. The rapid evolution after the first 10 ns corresponds to the enhanced adsorption stage, where for 2 ns, we use SMD to apply a gentle force on the IgG hydrophobic backbone that brings the protein closer to the substrate, intensifying the dehydration while keeping the internal structure intact. After this, the system equilibrates for another 140 ns.

the first 10 ns following the SMD step in which the IgG is brought into contact with the substrate, and shows that the dehydration/adsorption process occurs very fast. The variations observed in the evolution of the RMSD (shown in Fig. 3 for the *End*- and *Sideways*-on orientations) of the whole IgG backbone might seem to imply that equilibrium has not been reached. However, the analysis of the RMSD of the three individual domains, with variations below 1.5 Å after 60 ns of simulation, explains those fluctuations in terms of relative displacements of the different fragments around the extremely flexible *hinge* region that connects them, as previously reported for IgG embedded in water.[46] There is only one orientation, the *Sideway*-on one, where we can still observe some changes in the RMSD of one of the fragments even at the latest stages of the simulation. The RoG components provide an explanation: the non-absorbed Fab domain oscillates back and forth due to thermal fluctuations. This oscillation leads to a minor rearrangement of the atoms on the upper part of the Fc fragment, but does not affect to those in contact with the surface as shown by the evolution of the contact area, that remains constant through the whole oscillation process. This same orientation shows that our protocol for enhanced adsorption does not mask any important aspect of the process. One may legitimate worry about the system being locked in a metastable configuration that prevents any further evolution. After the enhanced adsorption in the *Sideway* orientation, there is a Fab in contact with the graphene layer. The analysis of the following MD steps reveals that this domain desorbs in order to reorient itself and, later on, adsorbs again but now along the paratope region.

The analysis presented so far proves that, using our adsorption protocol, 150 ns MD simulations are long enough to capture all of the relevant protein rearrangements involved in the adsorption process, and to reach the final stable equilibrium configuration for each IgG orientation. This analysis also supports one of the more striking results coming out from our simulations: in graphene, vertical orientations like *End*-on and *Sideway*-on, exposing the active Fab domains, seem to be stable adsorption configurations, at variance with previous findings on hydrophilic surfaces.[14–19]

The results of our MD simulations show that, at variance with the strong (complete) denaturation previously found for protein fragments,[31,34,35,47] small proteins like BMP-2[36] and larger proteins treated with implicit solvant methods,[37–42] the structure of the IgG is preserved during the adsorption process. The evolution of the secondary structure during the simulations, using both Ramachandran plots and the DSSP algorithm[48] (see Table 1 and Fig. S6–S9† for the different orientations), confirms that the IgG secondary structure is barely affected (fluctuations always smaller than 2%). Furthermore, in all of the orientations, the adsorbed residues have an even distribution of hydrophobic/hydrophilic residues. We do not observe any movement of residues belonging to the hydrophobic core/regions of the protein towards the surface as observed on smaller protein fragments.[33]

The results presented above clearly show that the role played by hydrophobic forces and the mechanisms governing protein adsorption for large proteins like IgG, with molecular weights around 150 kDa and high internal stability, are very different from the ones studied so far in protein fragments and smaller proteins.[33,35,36,44,47] The protein adsorption process is spontaneous only if there is a free energy gain upon adsorption ($\Delta G = \Delta H - T\Delta S < 0$), *i.e.* if the enthalpy energy variation due to adsorption (ΔH) is smaller than the entropic-energy variation ($T\Delta S$). In small proteins, the energy increase (ΔH) due to unfolding is small. As a result, the relative contribution of the entropic term to the overall free energy is more relevant. For this reason, small proteins or peptide chains easily unfold[33,35,36,44,47] over a hydrophobic surface such as graphene in order to minimize the disruption of the

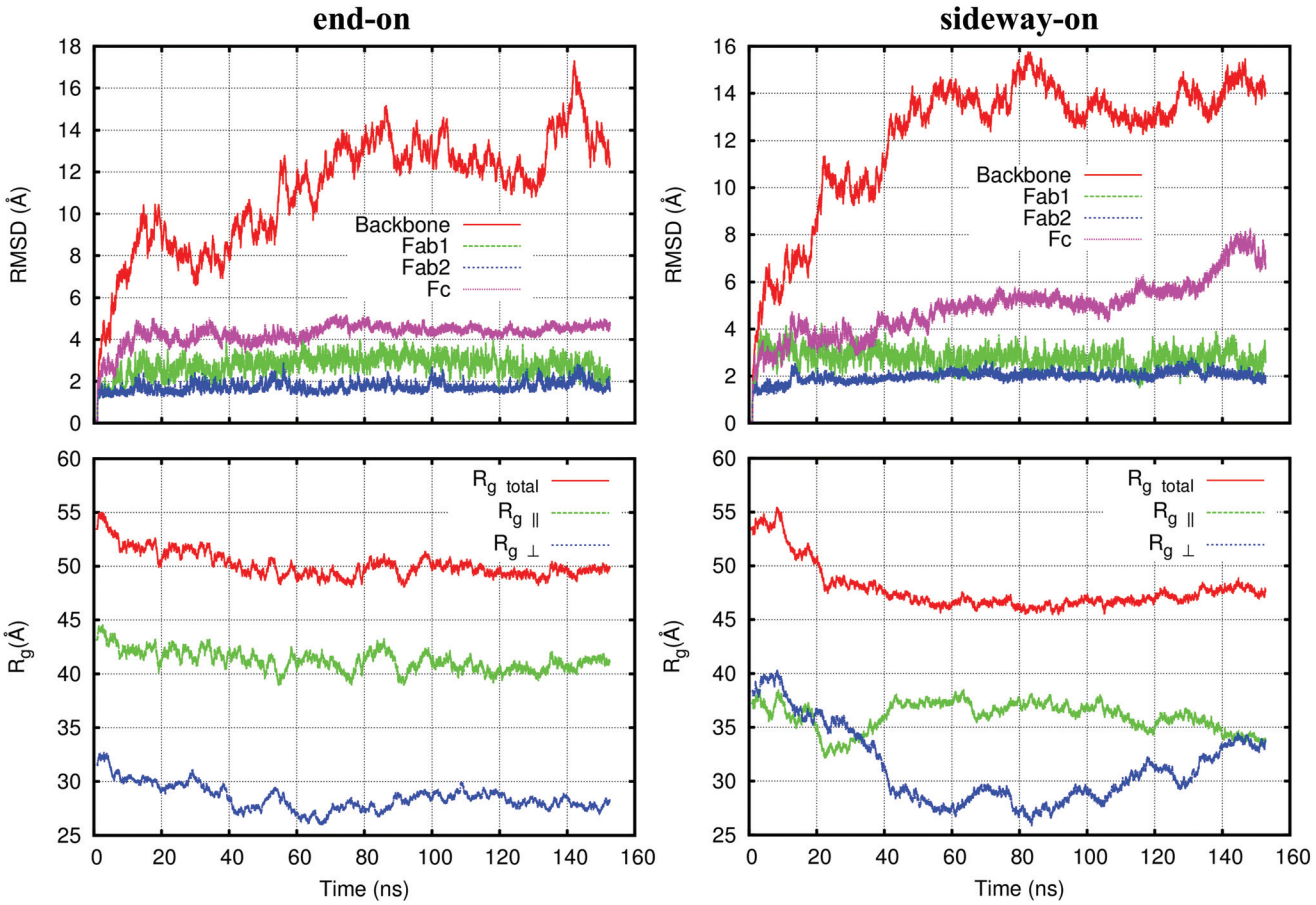

Fig. 3 Evolution during the adsorption dynamics of the root-mean-square deviation (RMSD) and the radius of gyration (R_g^2) for the *Sideway*- and *End*-on adsorption orientations. RMSD is calculated for the whole protein – all the backbone atoms of the protein (backbone) – and the alpha carbons belonging to each of the three domains, the two Fab (FAB1 and FAB2) and Fc domain (FC). The components $R_{g,||}^2$ and $R_{g,\perp} = (R_g^z)$ provide information on how the protein spreads over the surface or gets compact in the direction normal to it. Variations of RMSD and R_g^2 components in the last stages of the simulation correspond to the oscillation of IgG domains that are not adsorbed (see text). Corresponding data for the *Flat*- and *Head*-on orientations are shown in Fig. S4.†

Table 1 Secondary structure evolution over the adsorption dynamics (152 ns) along the *End* and *Sideway* orientations. Here we show the percentual value of each of the secondary structure component evaluated using the DSSP algorithm[48,49] at major simulation steps, *i.e.*: after the thermalization (stage A), after the 10 ns free adsorption dynamics (stage B), after the enhanced adsorption (stage C) and after the 140 ns free adsorption dynamics (stage D)

	End-on				*Sideway*-on			
Sec. Struct.	A	B	C	D	A	B	C	D
β-Strand	46.81	47.42	46.81	44.68	47.72	46.35	42.48	46.05
β-Bridge	1.37	1.14	1.37	1.22	1.29	1.82	2.20	1.22
α-Helix	3.50	3.65	2.96	2.13	3.57	3.42	2.96	1.98
3π-Helix	2.96	2.05	3.27	3.19	2.28	2.51	1.60	2.81
5π-Helix	0.00	00.00	00.00	00.00	00.00	00.00	00.00	00.00
Turn	11.09	12.16	11.40	12.31	11.93	11.09	13.60	12.84
Bend	9.65	9.19	9.95	10.33	9.35	10.18	10.33	10.26
Random-coil	24.62	24.39	24.24	26.14	23.86	24.62	26.82	24.85

water hydrogen bonding network. This allows the system to increase its entropy at a cost of a small unfolding energy barrier. For larger proteins, such as the IgG, this does not seem to be the case. Given the high internal stability of the IgG,[46,50,51] the enthalpy energy increase arising from the protein unfolding, or any major rearrangement, is too large to

be compensated by any entropic energy gain. Therefore neither we observe a rearrangement of the hydrophobic residues to favor their adsorption instead of the hydrophilic ones, nor we find a protein unfolding occurring upon adsorption.

AFM experiments for IgG adsorption

Our results regarding the preservation of the IgG structure and the presence of vertical orientations as stable adsorption configurations call for an independent validation. The capability of the AFM to directly visualize the behavior of biological molecules at solid–liquid interfaces enables to assess the MD simulations. The two right columns in Fig. 1 show high resolution Amplitude Modulation AFM (AM-AFM) images in the water of IgG antibodies deposited on graphene (panels c, g, k, o) and their corresponding cross-sections along the lines marked on the images (panels d, h, l, p). The lateral and vertical resolution of the images allows us to make a direct connection between protein configurations in theory and experiment. Furthermore, as time scales between AFM (100 ms) and MD (100 ns) are separated by six orders of magnitude, we completely overcome possible doubts about the long term stability of the structures found in the MD simulations.

The first important point is that the AM-AFM images reveal the four characteristic orientations of IgG on graphene as described by the MD simulations. A qualitative comparison between theory and experiments (panels a, e, i, m and c, j, k, o in Fig. 1 respectively) shows a good agreement between the theory-predicted and experimentally-observed adsorption orientations. In particular, we can identify the *Head*-on and *End*-on orientation. Fig. 1g (head-on orientation) clearly shows two protrusions of different heights: a lower one which corresponds to an adsorbed Fab fragment and a higher one corresponding to a Fab lying over the Fc fragment (blue line cross-section profile in Fig. 1h). On the other hand, for the *End*-on orientation, two protrusions of similar height are visible in Fig. 1k, and confirmed by the blue line in the cross-section profile in Fig. 1l. We have assigned these two protrusions to the Fab fragments exposed to the environment. This assignment is further confirmed by the inter-domain distances determined for these two orientations, as discussed below. It is worth mentioning that our AFM experiments are even able to distinguish between two configurations where the IgG lies flat on the surface. The *Flat*-180°-*xflipped* orientation (see Fig. S3†) is a specular reflection of the *Flat* configuration displayed in Fig. 1. In spite of the apparent equivalence of these two structures, our simulations show differences in their final adsorption structures. The Fc fragment is less strongly adsorbed in the *Flat* configuration. This fact, together with the torsional restrain imposed by the different adsorption of the Fab fragments, lifts the Fc domain upwards (see Fig. S3†). The height profiles in Fig. S3† confirm these differences, and demonstrate how powerful the synergy is between experiment and theory in order to have a detailed characterization and understanding of the mechanisms of adsorption.

The agreement goes beyond the similarities in shape and the ability to resolve different orientations, and it involves quantitative values. We observe that the measured inter-domain distances, extracted from AFM topography cross sections (like the ones shown in panels d, h, l and p of Fig. 1), are in agreement with the results from our MD simulations (see Table 2 and Fig. S5†). Note that, due to tip–antibody convolution effects, the overall size of the antibody is larger than the nominal value. However, distortion does not affect the inter-domain distances. Furthermore, these distances are also in agreement with reference data.[51] This quantitative agreement allows us, not only to validate the adsorption orientation mapping AFM-MD represented in Fig. 1, but also to confirm that the IgG retains its secondary structure when adsorbed over graphene.

The height comparison reveals some differences between experiment and theory. The experimental values are in the 3 to 3.5 nm range (Fig. 1d, h, l and p). For the *Flat* orientation, the maximum height value is also lower than the nominal height of the molecule (~6 nm). This is a common feature in AFM experiments and is due to the elastic deformation of the antibodies in the vertical direction by the force applied by the AFM probe during imaging. Numerical simulations[52] indicate that, for the operational values used here to image the proteins, the peak force is in the 400 pN range which implies deformations of about 2 nm for a system with an effective Young's modulus of 30 MPa. The deformation is enhanced for vertical orientations since they are softer along the direction perpendicular to the plane, due to the smaller effective *z*-atomic-density occurring in these orientations.

In order to gain further insight into the statistical distribution of the adsorption orientations of the IgG over graphene, we have performed a series of AFM measurements of IgG antibodies deposited on graphene. The orientations have been classified into three groups: flat, vertical and non-resolved. The flat group includes images that show the characteristic Y-shape of *Flat*-on orientation. The vertical one includes antibodies in *Head*-on, *Sideway*-on and *End*-on orientations. The flat orientations are recognized by the presence of three lobes (subunits) in the AFM image, while the vertical orientations are characterized by the presence of two lobes or one plus a protrusion nearby (see Fig. 1). The non-resolved group includes the images that show a geometry that did not

Table 2 Comparison of the inter-domain distances (in nm) as measured by AFM (columns 2 and 3) and by MD simulations (columns 4 and 5). The distances taken from the MD simulations were obtained from the coordinates at the end of the 152 ns equilibration run. Further details can be found in Fig. S5

	AFM		MD	
Orientation	Fab1–Fab2 (nm)	Fab–Fc (nm)	Fab1–Fab2 (nm)	Fab–Fc (nm)
Flat	9.4	5.8	9.3	8.8
Flat-180°-*xflipped*	9.6	10.0	9.3	8.7
Head	—	9.7	—	9.3
End	8.0	—	8.0	—

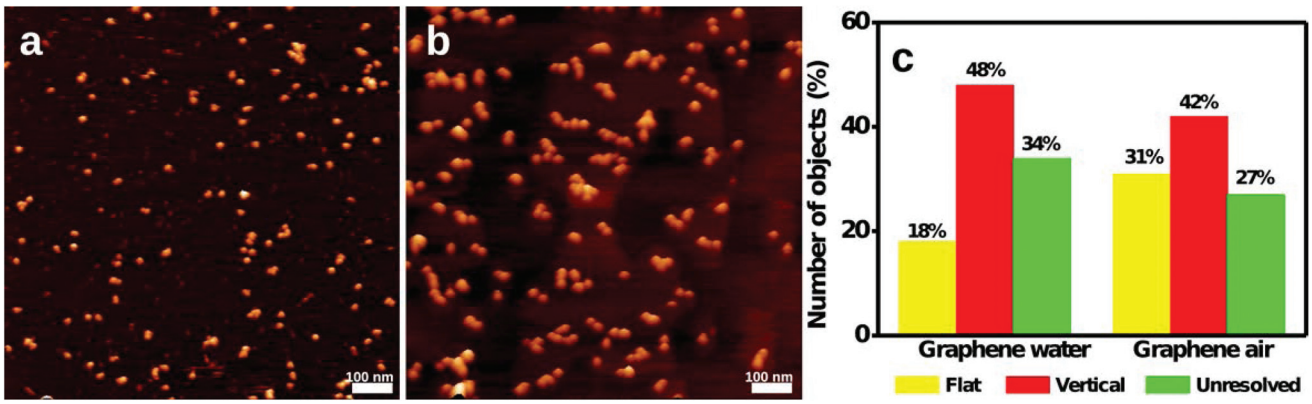

Fig. 4 a. AM-AFM topographic image of the IgG adsorbed on graphene (water). b. AM-AFM topographic image of the IgG adsorbed on graphene (air). c. Histogram with the number of counts (in percentage values) of antibodies adsorbed along a *Flat* orientation (*i.e. Flat*-on and *Flat*-180°-x*flipped*), along a vertical orientation (*i.e. Head*, *Sideway*, and *End*) and for the unresolved orientations. The total number of counts in water is 145 and in air is 385.

match any of the orientations given by the MD simulations. This happens when two antibodies are very close on the substrate or when the subunits have not been resolved by the AFM. All these orientations were categorized by analyzing several 500 × 500 nm^2 images of antibodies on graphene similar to the ones shown in Fig. 4a and S10.† The histogram in Fig. 4c shows that the IgGs adsorb mostly on vertical orientations (*i.e. Head*-on, *Sideway*-on, *End*-on). This is in contrast with the results obtained in the hydrophilic surfaces (including mica, silica and quartz) studied so far.[14–19] All of these passive adsorption surfaces favor the non-bioactive *Flat* adsorption orientation for the low coverage densities considered in this work. The dominant presence of vertically oriented IgGs is fully consistent with the fact that, according to our MD simulations, all the studied orientations are stable adsorption states. We have also performed similar experiments in air (Fig. 4b) to see whether or not the dehydration process could introduce some changes in the dominant orientations. Although there are differences in the relative percentages of the *Flat*-on and unresolved orientations, our results in air clearly show that, as in the water case, the vertical orientation is still the dominant one.

Understanding the statistical distribution of orientations: SMD simulations for the desorption process

In order to understand the origin of the statistical distribution obtained in the AFM experiments, we have performed SMD simulations for the IgG desorption process, as represented in Fig. 5. Using the Jarzynski equality,[53] the free energy difference between two equilibrium states can be obtained by an exponential average of the work needed to take the system from one state to the other (*e.g.*, from adsorbed to desorbed IgG) *via* any desired non-equilibrium process. The average has to be done over multiple initial configurations/coordinates sampled from the initial equilibrium state. This method, previously used to measure the adsorption energy of a peptide onto different hydrophobic surfaces,[32] provides results which are in excellent agreement with those obtained from AFM force spectroscopy (accuracy higher than 5 pN). In our case, we have performed a SMD by applying a constant force to the same 30 S-bonded cysteine alpha carbons used in the SMD for the enhanced adsorption (see Methods and Fig. S2†). These atoms, evenly distributed along the protein backbone, allow us to rigidly fix the protein structure and thus measure only the cost of adsorption, and not any possible reconstruction occurring during the desorption process. Note that this set of atoms is the same as the one used during the SMD procedure to force the adsorption of the molecule onto the surface. The pulling velocity (2.5 Å ns^{-1}) and the harmonic restrains (50 kcal mol^{-1}) have been chosen to assure a smooth desorption process (so forces on each step are very close to the potential-mean-force curve) and a stable adsorption energy (no work is required after the full desorption stage is reached).

This procedure has been applied to calculate the adsorption free energy of the IgG on graphene along the *Flat*-on and *Sideway*-on orientations. The exponential averages include 15 independent SMDs per orientation, with the initial coordinates sampled every 2 ns from the last 30 ns of simulations. Given the high computational cost of these simulations, we have carefully explored the maximum deviation (δW) of each individual work curve to the Jarzynski average for these two orientations. As shown in Fig. 5, δW is less than 7% of the total energy. Based on these results, for the other two orientations, *Head* and *End*, we have evaluated the total desorption work curve by using only a single SMD run.

The free energies of adsorption obtained for the orientations *Flat*, *Head*, *Sideway* and *End* are 685, 503, 359 and 325 kcal mol^{-1}, respectively. Interestingly, a plot of the adsorption energy *versus* the contact area for all the orientations reveals a linear dependence with a ratio of 0.28 ± 0.016 kcal mol^{-1} $Å^{-2}$. This ratio compares very well with the value of 0.30 kcal mol^{-1} $Å^{-2}$ that can be estimated from the binding energies obtained with the gold standard in computational chemistry, CCSD calculations, for a large test set of complexes

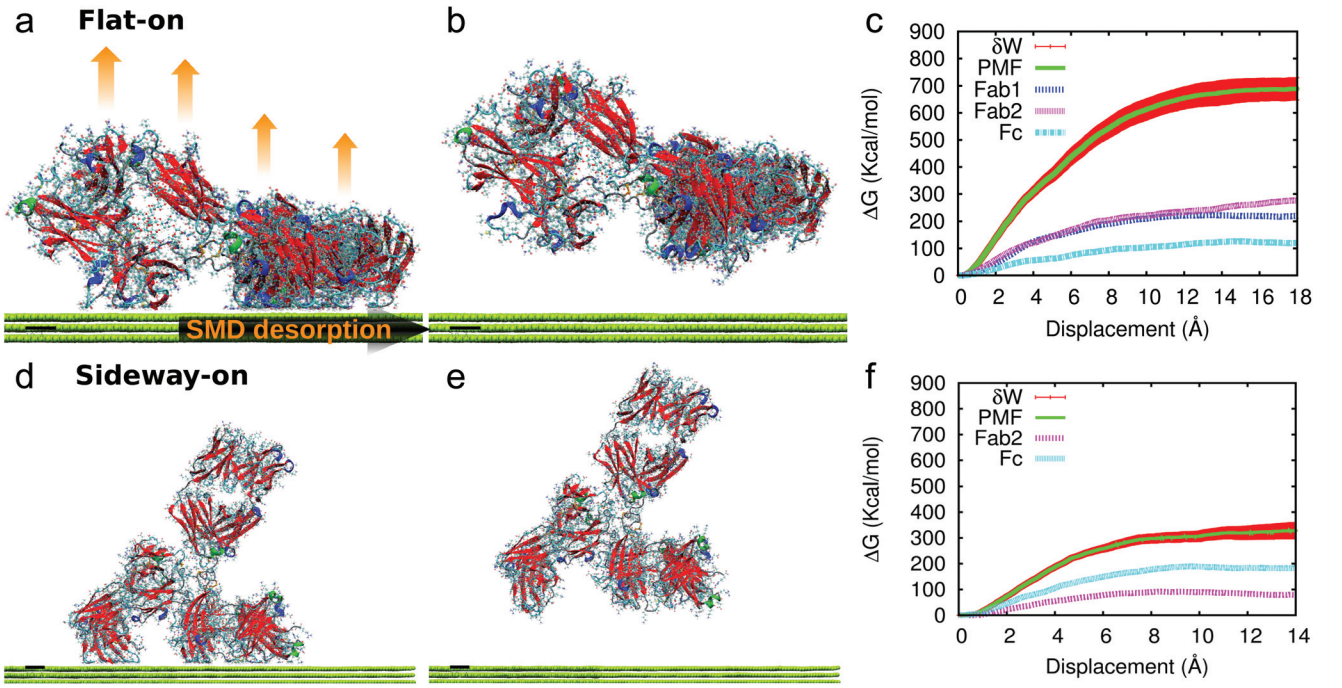

Fig. 5 Adsorption energies calculated from steered MD simulations. (a) Side view of an IgG adsorbed along the *Flat* orientation after 138 ns MD simulation. The secondary structure IgG is represented using the same convention as in Fig. 1. Superimposed, we have added a translucent ball-and-stick model representation of all of the atoms in the protein. (b) Side view of the IgG after one of the 15 SMD desorption simulations. (c) Free energy evolution along the desorption process averaged over 15 SMD simulations. We represent the maximum deviation (δW) for all the 15 SMD work curves (red) with respect to the Jarzynski exponential average (Potential–Mean–Force – PMF, green). The curves labelled as Fab1, Fab2, and Fc represent the PMF for each of these domains calculated separately. (d)–(e) The same results are obtained for the *Sideway* orientation. Note that PMF curves are constant for displacements larger than 10–12 Å, indicating that the IgG–graphene interaction has already vanished and, thus, no further work is required to move the IgG apart from the surface.

interacting mostly *via* London-dispersion forces.[54] This agreement not only confirms that our adsorption energies are sound (adequate), but it also reinforces the argument that the forces governing the adsorption of large proteins like the IgG arise mostly from van der Waals (vdW) interactions, while hydrophobic forces seem to play a very minor role.

These large adsorption energies provide the clue for the observation of the different adsorption orientations. All of them have adsorption energies that are much higher than the total IgG unfolding energy barrier ~165–265 kcal mol^{-1}.[50] If enough thermal energy were available, it would be energetically less costly for the IgG to unfold than to desorb. As both theory and experiments undoubtedly show that the IgG retains its secondary structure when adsorbed over graphene, it follows that this is not the case. In order to change its adsorption orientation, the IgG must first desorb (partially or totally) from the surface. Given that the thermal energy available is smaller than the high energy barriers required for this process to occur, once the IgG gets adsorbed along a given orientation, it will not naturally desorb nor change its orientation. As discussed above, the similarity between air and water AFM measurements, shows that entropic thermal fluctuations, enhanced in the water measurements, are not large enough to affect the final adsorption state and change this scenario. The picture that emerges for the adsorption process is as follows: initially, the IgG is freely drifting on the solvent until it reaches the surface along any of the 6 possible molecular orientations (*Flat*, *Head*, *Sideway*, *End*, and the other two equivalent orientations, *i.e.* *Flat*-180°-*xflipped* and *Sideway*-180°-*xflipped* – see Fig. S1†). Then, already in close contact with the surface, it starts to adsorb along its particular landing orientation. Once the adsorption process starts, given its speed and the high adsorption energies, the antibody gets anchored to the surface along the landing orientation. As a result, the final adsorption orientation is determined by the essentially random landing orientation, *i.e.* each of the six orientations have an equal probability of being found over the graphene surface. The statistics obtained in our experiments support this description. Not considering the unresolved orientations, we observe that in water 27% of the antibodies adsorb on a *Flat* orientation (*i.e.*, *Flat* and *Flat*-180°-*xflipped*), which is in good agreement with the probability of (2/6) × 100 = 33.3% predicted for randomly landing on this orientation.

Single molecule force spectroscopy (SFS) on graphene

The immunological activity of the deposited antibodies has been assessed by SFS.[55–57] The experiments involve the measurement of the rupture forces existing between the IL-4

cytokine (antigen) attached to the AFM tip and the anti-IL4 antibodies[58] immobilized on the graphene substrate. Fig. 6a shows a distribution of anti-IL4 antibodies on graphene and Fig. 6b shows the corresponding force curves obtained on the four antibodies marked in Fig. 6a. To illustrate the specific character of the interactions between the antibody and its specific antigen we also plot two force curves obtained on two locations where the AFM image does not show any antibody.

A rigorous validation of the immunological response by SFS requires a statistical analysis of thousands of force curves. The SFS data interpretation could be hampered by the presence of both unspecific and multiple simultaneous unbinding events. An efficient way to reduce their contribution to the overall statistics is by limiting the likelihood of bond formation upon tip–sample contact. We have adjusted the experimental parameters to obtain a 14% specific binding probability, which implies that the majority of the recorded events are single molecular

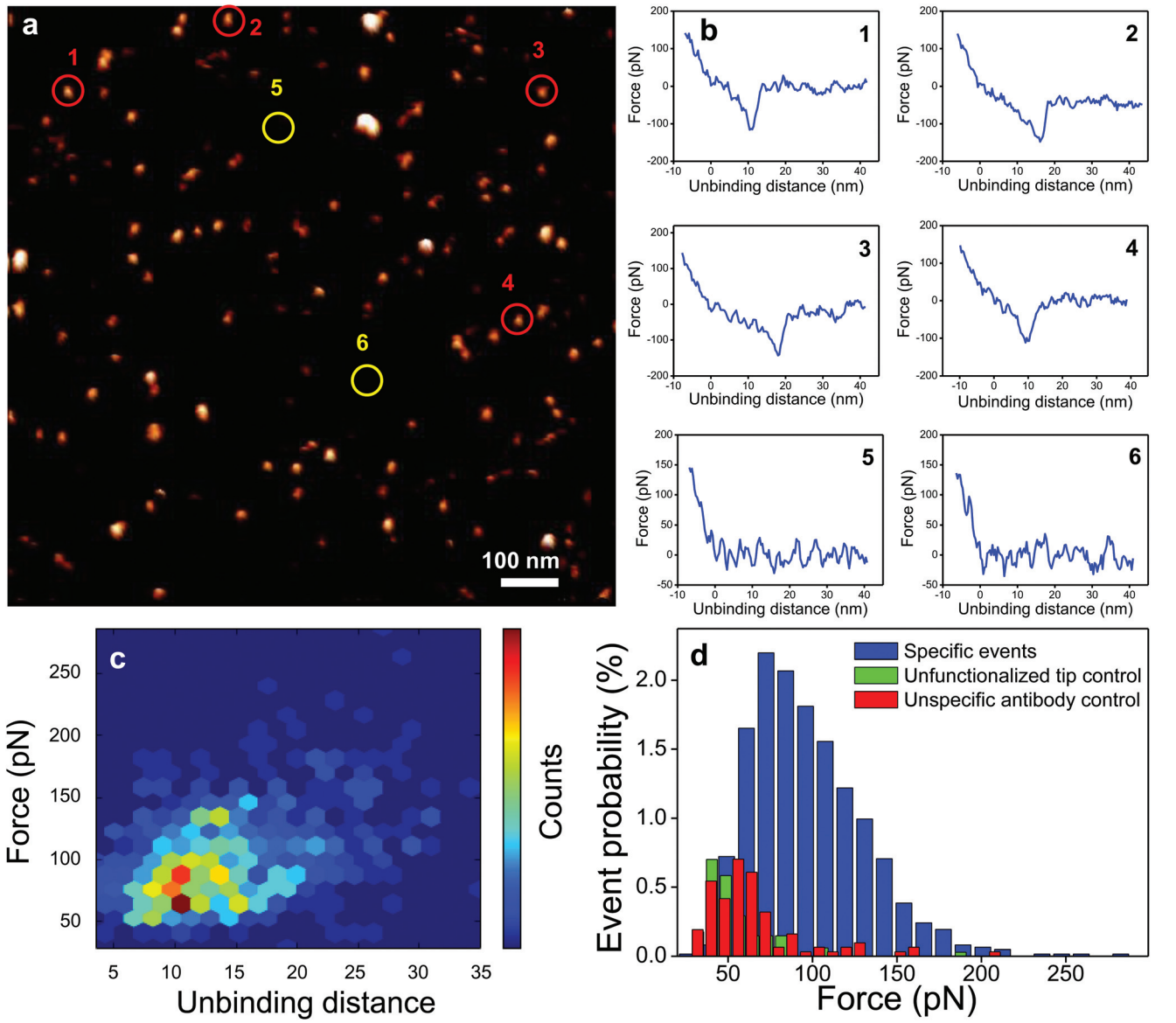

Fig. 6 Single molecule force spectroscopy on graphene. (a) Topography and adhesion force AFM image of anti-IL4 antibodies on graphene. A force *versus* distance curve is acquired at each pixel of the image, while maintaining the *x* and *y* positions constant. The circles indicate the positions of the force curves illustrated on b. (b) Force *versus* distance curves measured on the positions marked in (a). 1–4 correspond to positions where antibodies are located in the AFM image while 5–6 correspond to locations with no antibodies. The topography image and the force curves were obtained by applying forces below 150 pN. Each force curve comprises 153 points and was taken with a tip velocity of 9.4 μm s^{-1}. (c) Molecular recognition map on the IL-4 and anti-IL-4 antibodies. The map plots the rupture forces with the corresponding unbinding distances. (d) Histogram of rupture forces the immunological detection and two control experiments on graphene. The statistics (percentages) consider all the events recorded by the force curves (specific and non-specific). However, the histogram only includes the events that meet the requirements to be considered as specific.

recognition interactions.[59] Fig. 6c shows the two dimensional molecular recognition map obtained on graphene.[58] This requires to implement a different methodology than the one illustrated in Fig. 6b. For example, the graphene surface is fully covered with IgGs to maximize the probability of antibody–antigen recognition events. In addition, each force curve has about 10 000 data points to properly identify the rupture events. The map shows the most probable rupture force between IL-4 and anti-IL4 happens at 75 pN and involves an unbinding length of 11 nm.

We have performed additional control experiments by changing the conjugation of the silicon tips. Fig. 6d shows the probability of finding a specific immunological recognition event as a function of the rupture force in comparison with the data obtained with a bare silicon tip and with a tip functionalized with an antigen (IL-6 cytokine) that does recognize the anti-IL4 antibody. The rupture forces in the absence of immunological recognition are smaller and the number of events are also significantly smaller. The smaller value of the force indicates its unspecific character. From all of the above we conclude that antibodies deposited on graphene retain their biological activity.

Conclusions

In summary, we have combined molecular dynamics simulations and high resolution AFM imaging to understand the adsorption of antibodies on graphene, considering it as a model for a hydrophobic surface. Our calculations for different orientations prove that the IgGs are strongly bound to graphene and that free energies of adsorption are proportional to the contact area. This result, together with the absence of any significant rearrangement of the residues belonging to the hydrophobic core towards the substrate, shows that the adsorption of large proteins like the IgG is dominated by vdW interactions, while hydrophobic forces seem to play a very minor role. This scenario is radically different from what previous simulations have shown for the adsorption of protein fragments and small proteins on hydrophobic surfaces. We conclude that the protein adsorption and the changes in the protein structure are size-dependent processes, where the internal strength of the protein plays a crucial role in the energy balance. Therefore, it is not possible to assess the host-response of a given material with the adsorption of just small protein fragments. Finally, we observe that the most abundant adsorption orientations, even at low IgG coverage densities, are the vertical ones. This is a particularly relevant result since on all passive-adsorption surfaces studied so far, the IgG adsorbs preferentially in *Flat* orientations, where the Fab domains are no longer easily accessible and, therefore, the IgG may lose some of its bioactivity once it is adsorbed. Thus, the key properties necessary to develop very sensitive immunological sensors – preservation of the secondary structure, strong protein anchoring, vertical adsorption orientations, and immunological recognition – arise from the simple deposition of the IgG of graphene without any complex surface functionalization protocol, making graphene an attractive substrate for immunosensing.[60,61]

Methods

MD simulations

The protein structure of the Immunoglobulin G (IgG), composed of 1316 amino acids and 2 glycan heteropolymer chains, was obtained from the protein data bank (PDBID: 1IGT[51]). The overall protonation state corresponds to a pH of 7.6 and a zero net charge. The IgG was then placed on top of a 20×20 nm^2 three-layer graphene slab with A–B–A stacking. The bottom layer of the slab was kept fixed during the simulations. The system was solvated with a cubic box of TIP3P water molecules[45] with a 10 Å buffer of solvent between the solvent and the furthest dimension in each direction. In total, we have 12 946 atoms in the protein, 47 019 in the slab representing the substrate, and, depending on the IgG orientation, from 385 257 to 709 248 atoms in the water solvent. The protein and the oligosaccharide were modeled by the AMBER's ff99SB[62] and Glycam04[63] force fields respectively. The choice of these force-fields was motivated by a previous study, in which it was reported[46] that these force-fields successfully sample the conformational space that an antibody explores in aqueous solution. The carbon atoms of the three-layered graphene were modeled by the OPLS aromatic carbon force field present on AMBER's generalized AMBER force-field.[64] These force fields are known to accurately reproduce graphene/graphite mechanical and hydration properties.[36,65]

All the simulations were performed using AMBER software suite.[66] In particular, the MD simulations were carried out using AMBER's PMEMD with NVIDIA GPU acceleration.[67] Production MD simulations were carried out at a constant temperature of 300 K ensured by a Langevin thermostat. A constant pressure of 1 atm was applied during the thermalization state. Given the higher computational cost of a NPT simulation, and also that it is reasonable to assume that the system pressure should remain unaltered during the adsorption process, during the production runs (the ones following thermalization) we have kept the volume fixed. The time step for integrating the equations of motion was set to 2 fs and the SHAKE algorithm was used in all of the simulations. The Particle–Mesh–Ewald summation was used to calculate long range electrostatic interactions. The cutoff for the van der Waals interaction was set to 10 Å. All the simulations were carried out on 6 GPUs per orientation, summing up a total of more than one million hours of CPU time.

Steered-molecular-dynamics (SMD) simulations were used at two different stages: initially to enhance the protein adsorption (in the time interval 10–12 ns), and at the end in order to compute desorption free energies. In both cases, the only SMD parameters that one can control are: the group of atoms to which the force is applied, the velocity of the SMD, and the spring constant of the applied force. These parameters were

considered *converged* once all the following requirements were met: not to produce any structural rearrangement on the IgG, and to yield a stabilization (with null variation) of the desorption free-energy curve once the protein is far from the surface. The set of parameters that satisfied all these requirements were: all the 30 S-bounded cysteine alpha carbons represented in Fig. S2,† $||\tilde{v}||$ = 0.25 ms^{-1}, and a spring constant of 50 kcal mol^{-1} $Å^{-1}$. The desorption free energies of the *Flat* and *Sideway* IgG orientations were obtained *via* an exponential average (*i.e.* using the Jarzynski equality[53]) of the work curves obtained in 15 independent SMDs with starting configurations sampled every 2 ns from the last 30 ns of simulation. The desorption free energies of the *Head* and *End* orientations were obtained *via* a single work curve obtained by performing a single SMD with the initial atomic coordinates extracted from the 150th ns of the simulation.

AFM imaging

The experiments were performed by amplitude modulation atomic force microscopy (AM-AFM)[68] using a Cypher AFM (Asylum Research, Oxford Instruments). For the experiments in water, we have used cantilevers (biolever fast, Olympus) with a force constant, driving frequency and quality factor of 100 pN nm^{-1}, 307.60 kHz, and 1.4, respectively. The free and set point amplitudes were 3.8 nm and 2.8 nm. For the experiments in air, we have used cantilevers (Supersharp silicon tips, Nanosensors) with a force constant, driving frequency and quality factor of 35 N m^{-1}, 310 kHz, and 280. The free and set point amplitudes were 8 nm and 7.5 nm.

Graphene

Graphene layers were generated by repeatedly cleaving Kitsh graphite with adhesive tape. The graphene flakes adhered to the tape were transferred by a applying a gentle mechanical contact between the tape and a freshly cleaved piece of mica.[69]

Antibodies

The antibodies were purchased from Sigma Aldrich (product id. A6029). They were prepared from a concentrated solution and then diluted 1 : 500 to 1 : 1000 times and deposited over the graphene substrate for 20 s; the sample was rinsed with water. The deposition protocol is identical for air and water experiments. For the experiments performed in air, once the antibodies have been deposited, the sample is dried by blowing dry nitrogen and imaged in air.

Single molecule force spectroscopy

Single molecule force spectroscopy experiments were performed at room temperature with a JPK Nanowizard III microscope (JPK Instruments, Germany). Triangular silicon nitride cantilevers with a nominal spring constant of 0.02 N m^{-1} and resonant frequency of 2 kHz were used. The force constant and quality factor are determined by using the thermal noise method.[70,71] At the end of each experiment, the optical lever sensitivity was calibrated by acquiring deflection *versus* distance curves on a hard surface (mica). Typically 100 deflection *versus* distance curves were acquired and the sensitivity of the photodiode was calculated as the mean value of the slope of the deflection curve measured in the repulsive region. The force was calculated by using Hooke's law, (Δz is the cantilever deflection, k is the cantilever force constant). The maximum force was maintained below 250 pN to avoid any irreversible damage to the molecules bound to the tip apex. For each functionalized tip, several force maps covering 1 μm × 1 μm regions of the sample (32 × 32 data points) were acquired. In each force curve, the tip was approached and retracted 100 nm from the sample at a speed of 200 nm s^{-1} and it was kept in contact with the sample for 0.5 s to facilitate the formation of antibody–antigen complexes.

Tip functionalization

PBS, 3-aminopropyl-triethoxysilane (APTES), sulphuric acid and ethanol were purchased from Sigma Aldrich (Madrid, Spain). The NHS-PEG24-Mal heterobifunctional linker and the sulfhydryl addition kit containing: SATA (N-succinimidyl-*S*-acetylthioacetate), hydroxylamine–HCl, conjugation buffer stock (10×) and dimethylformamide were purchased from Thermo Fisher Scientific (Madrid, Spain). Monoclonal anti-murine IL-4 (antibody) and recombinant murine IL-4 (antigen) were purchased from Biovision (San Francisco, USA).

The antigen was attached to the AFM tip *via* a heterobifunctional flexible spacer, as described previously.[58] Briefly, triangular silicon nitride cantilevers (OTR4, Brucker, Santa Barbara) were first cleaned by immersion in a solution of 0.25 M sulphuric acid–9.8 M hydrogen peroxide 4 : 1 v/v for 30 minutes. After rinsing with ultrapure water, the cantilevers were immersed into a solution of APTES–water–ethanol 5 : 5 : 90 v/v for 30 minutes. The resulting amino-functionalized tips were then rinsed with ultrapure water and ethanol, dried with nitrogen gas and stored in a dry atmosphere.

The next step involved the addition of free sulfhydryl groups to the IL-4 antigen. To do so, a 10-fold molar excess of an 8.65 mM SATA solution in DMF was added to the antigen solution and the reaction was incubated for 30 minutes at room temperature. To de-protect the latent sulfhydryl groups, 2.5 μl of a 50 mg ml^{-1} hydroxylamine–HCl in conjugation buffer stock solution (10×) was added to the SATA-modified antigen solution and the mixture was incubated for 2 hours at room temperature. The PEG linker in 10-fold molar excess was coupled to the modified antigen molecule by incubation at 4 °C overnight. Finally, the amino-functionalized AFM tips were immersed in the PEG-antigen solution for 2 hours at room temperature. The tips were rinsed with PBS 0.01 M and stored in a Petri dish at 4 °C until further use.

Acknowledgements

We thank the financial support from the Spanish MINECO (projects Consolider Force-For-Future CSD2010-00024, MAT2011-023627, MAT2013-44858-R, FIS2012-36113-C03-03, and MAT2014-54484-P), and from Comunidad de Madrid

(S2009/MAT-1467). The authors thankfully acknowledge the computer resources, technical expertise and assistance provided by the Red Española de Supercomputación at the Minotauro Supercomputer (BSC, Barcelona). We also acknowledge the support provided by the computing facilities of the Extremadura Research Centre for Advanced Technologies (CETA-CIEMAT), funded by the European Regional Development Fund (ERDF). CETA-CIEMAT belongs to CIEMAT and the Government of Spain.

References

1 W. Norde, T. A. Horbett and J. L. Brash, *Proteins at Interfaces III State of the Art*, American Chemical Society, 2012, vol. 1120, pp. 1–34.
2 W. R. Sanhai, J. H. Sakamoto, R. Canady and M. Ferrari, *Nat. Nanotechnol.*, 2008, **3**, 242–244.
3 Z. Zhang, M. Zhang, S. Chen, T. A. Horbetta, B. D. Ratner and S. Jiang, *Biomaterials*, 2008, **29**, 4285–4291.
4 D. G. Castner and B. D. Ratner, *Surf. Sci.*, 2002, **500**, 28–60.
5 A. A. Yanik, M. Huang, O. Kamohara, A. Artar, T. W. Geisbert, J. H. Connor and H. Altug, *Nano Lett.*, 2010, **10**, 4962–4969.
6 Z. Wu, H. Chen, X. Liu and J. L. Brash, *Macromol. Biosci.*, 2012, **12**, 126–131.
7 T. Abramyan, G. Collier, T. G. Kucukkal, X. Li, J. A. Snyder, A. A. Thyparambil, N. A. Vellore, Y. Wei, J. A. Yancey, S. J. Stuart and R. A. Latour, *Proteins at Interfaces III State of the Art*, American Chemical Society, 2012, vol. 1120, pp. 197–228.
8 A. E. Nel, L. Mdler, D. Velegol, T. Xia, E. M. V. Hoek, P. Somasundaran, F. Klaessig, V. Castranova and M. Thompson, *Nat. Mater.*, 2009, **8**, 543–557.
9 L. Beaudet, R. Rodriguez-Suarez, M.-H. Venne, M. Caron, J. Bdard, V. Brechler, S. Parent and M. Bielefeld-Svigny, *Nat. Methods*, 2008, **5**, an8-an9.
10 E. Sevier, *J. Med. Technol.*, 1985, **2**, 287–293.
11 J. Tamayo, P. M. Kosaka, J. J. Ruz, A. S. Paulo and M. Calleja, *Chem. Soc. Rev.*, 2013, **42**, 1287–1311.
12 J. B. Lyczak and G. B. Pier, *Immunology, infection, and immunity*, ASM Press, Washington, DC, 2004.
13 R. Jefferis, J. Lund and J. D. Pound, *Immunol. Rev.*, 1998, **163**, 59–76.
14 X. Zhao, M. Yaseen, F. Pan and J. R. Lu, *Proteins at Interfaces III State of the Art*, American Chemical Society, 2012, vol. 1120, pp. 543–574.
15 C. Dupont-Gillain, *Proteins at Interfaces III State of the Art*, American Chemical Society, 2012, vol. 1120, pp. 453–469.
16 N. Tajima, M. Takai and K. Ishihara, *Anal. Chem.*, 2011, **83**, 1969–1976.
17 J. R. Lu, X. Zhao and M. Yaseen, *Curr. Opin. Colloid Interface Sci.*, 2007, **12**, 9–16.
18 X. Zhao, F. Pan and J. R. Lu, *J. R. Soc., Interface*, 2009, **6**, S659–S670.
19 H. Xu, J. R. Lu and D. E. Williams, *J. Phys. Chem. B*, 2006, **110**, 1907–1914.
20 J. Preiner, N. S. Losilla, A. Ebner, P. Annibale, F. Biscarini, R. Garcia and P. Hinterdorfer, *Nano Lett.*, 2009, **9**, 571–575.
21 S. Ido, H. Kimiya, K. Kobayashi, H. Kominami, K. Matsushige and H. Yamada, *Nat. Mater.*, 2014, **13**, 264–270.
22 Y. Zhang, T. R. Nayak, H. Hong and W. Cai, *Nanoscale*, 2012, **4**, 3833–3842.
23 X. Hu and Q. Zhou, *Chem. Rev.*, 2013, **113**, 3815–3835.
24 T. Alava, J. A. Mann, C. Thodore, J. J. Benitez, W. R. Dichtel, J. M. Parpia and H. G. Craighead, *Anal. Chem.*, 2013, **85**, 2754–2759.
25 A. San Paulo and R. Garcia, *Biophys. J.*, 2000, **78**, 1599–1605.
26 S. Patil, N. F. Martinez, J. R. Lozano and R. Garcia, *J. Mol. Recognit.*, 2007, **20**, 516–523.
27 D. Martinez-Martin, E. T. Herruzo, C. Dietz, J. Gomez-Herrero and R. Garcia, *Phys. Rev. Lett.*, 2011, **106**, 198101.
28 R. C. Chaves, J.-M. Teulon, M. Odorico, P. Parot, S.-W. W. Chen and J.-L. Pellequer, *J. Mol. Recognit.*, 2013, **26**, 596–604.
29 F. Kienberger, H. Mueller, V. Pastushenko and P. Hinterdorfer, *EMBO Rep.*, 2004, **5**, 579–583.
30 R. C. Chaves and J.-L. Pellequer, *Bioinformatics*, 2013, **29**, 3230–3231.
31 J. Katoch, S. N. Kim, Z. Kuang, B. L. Farmer, R. R. Naik, S. A. Tatulian and M. Ishigami, *Nano Lett.*, 2012, **12**, 2342–2346.
32 D. Horinek, A. Serr, M. Geisler, T. Pirzer, U. Slotta, S. Q. Lud, J. A. Garrido, T. Scheibel, T. Hugel and R. R. Netz, *Proc. Natl. Acad. Sci. U. S. A.*, 2008, **105**, 2842–2847.
33 T. Wei, M. A. Carignano and I. Szleifer, *Langmuir*, 2011, **27**, 12074–12081.
34 G. Zuo, X. Zhou, Q. Huang, H. Fang and R. Zhou, *J. Phys. Chem. C*, 2011, **115**, 23323–23328.
35 L. Ou, Y. Luo and G. Wei, *J. Phys. Chem. B*, 2011, **115**, 9813–9822.
36 C. Mücksch and H. M. Urbassek, *PLoS One*, 2013, **8**, e64883.
37 G. Raffaini and F. Ganazzoli, *Langmuir*, 2013, **29**, 4883–4893.
38 C. Mücksch and H. M. Urbassek, *Langmuir*, 2011, **27**, 12938–12943.
39 C. Mücksch and H. M. Urbassek, *Chem. Phys. Lett.*, 2011, **510**, 252–256.
40 G. Raffaini and F. Ganazzoli, *Langmuir*, 2010, **26**, 5679–5689.
41 G. Raffaini and F. Ganazzoli, *Macromol. Biosci.*, 2007, **7**, 552566.
42 F. Ganazzoli and G. Raffaini, *Phys. Chem. Chem. Phys.*, 2005, **7**, 3651.
43 Y. Sun, B. N. Dominy and R. A. Latour, *J. Comput. Chem.*, 2007, **28**, 1883–1892.
44 T. Wei, M. A. Carignano and I. Szleifer, *J. Phys. Chem. B*, 2012, **116**, 10189–10194.

45 W. L. Jorgensen, J. Chandrasekhar, J. D. Madura, R. W. Impey and M. L. Klein, *J. Chem. Phys.*, 1983, **79**, 926–935.
46 J. P. Brandt, T. W. Patapoff and S. R. Aragon, *Biophys. J.*, 2010, **99**, 905–913.
47 C.-C. Chiu, G. R. Dieckmann and S. O. Nielsen, *J. Phys. Chem. B*, 2008, **112**, 16326–16333.
48 W. Kabsch and C. Sander, *Biopolymers*, 1983, **22**, 2577–2637.
49 R. P. Joosten, T. A. te Beek, E. Krieger, M. L. Hekkelman, R. W. Hooft, R. Schneider, C. Sander and G. Vriend, *Nucleic Acids Res.*, 2011, **39**, D411–D419.
50 A. W. P. Vermeer and W. Norde, *Biophys. J.*, 2000, **78**, 394–404.
51 L. J. Harris, S. B. Larson, K. W. Hasel and A. McPherson, *Biochemistry*, 1997, **36**, 1581–1597.
52 H. V. Guzman, A. P. Perrino and R. Garcia, *ACS Nano*, 2013, **7**, 3198–3204.
53 C. Jarzynski, *Phys. Rev. Lett.*, 1997, **78**, 2690–2693.
54 P. Jurecka, J. Sponer, J. Cerny and P. Hobza, *Phys. Chem. Chem. Phys.*, 2006, **8**, 1985–1993.
55 P. Hinterdorfer, W. Baumgartner, H. J. Gruber, K. Schilcher and H. Schindler, *Proc. Natl. Acad. Sci. U. S. A.*, 1996, **93**, 3477–3481.
56 A. R. Bizzarri and S. Cannistraro, *Nanotechnology*, 2014, **25**, 335102.
57 A. Noy and R. W. Friddle, *Methods*, 2013, **60**, 142–150.
58 S. Casalini, A. C. Dumitru, F. Leonardi, C. A. Bortolotti, E. T. Herruzo, A. Campana, R. F. de Oliveira, T. Cramer, R. Garcia and F. Biscarini, *ACS Nano*, 2015, **9**, 5051–5062.
59 E. Evans and P. Williams, in *Physics of bio-molecules and cells. Physique des biomolécules et des cellules: Session LXXV. 2–27 July 2001*, ed. F. Flyvbjerg, F. Jülicher, P. Ormos and F. David, Springer Berlin Heidelberg, Berlin, Heidelberg, 2002, ch. Dynamic Force Spectroscopy, pp. 145–204.
60 M. Pumera, *Mater. Today*, 2011, **14**, 308–315.
61 T. Kuila, S. Bose, P. Khanra, A. K. Mishra, N. H. Kim and J. H. Lee, *Biosens. Bioelectron.*, 2011, **26**, 4637–4648.
62 K. Lindorff-Larsen, S. Piana, K. Palmo, P. Maragakis, J. L. Klepeis, R. O. Dror and D. E. Shaw, *Proteins: Struct., Funct., Bioinf.*, 2010, **78**, 1950–1958.
63 K. N. Kirschner, A. B. Yongye, S. M. Tschampel, J. Gonzlez-Outeirio, C. R. Daniels, B. L. Foley and R. J. Woods, *J. Comput. Chem.*, 2008, **29**, 622–655.
64 J. Wang, R. M. Wolf, J. W. Caldwell, P. A. Kollman and D. A. Case, *J. Comput. Chem.*, 2004, **25**, 11571174.
65 J.-L. Tsai and J.-F. Tu, *Mater. Des.*, 2010, **31**, 194–199.
66 *AMBER12*, 2012, http://ambermd.org/.
67 R. Salomon-Ferrer, A. W. Gtz, D. Poole, S. Le Grand and R. C. Walker, *J. Chem. Theor. Comput.*, 2013, **9**, 3878–3888.
68 R. Garcia and A. San Paulo, *Phys. Rev. B: Condens. Matter*, 1999, **60**, 4961–4967.
69 R. Mas-Balleste, C. Gomez-Navarro, J. Gomez-Herrero and F. Zamora, *Nanoscale*, 2011, **3**, 20–30.
70 J. L. Hutter and J. Bechhoefer, *Rev. Sci. Instrum.*, 1993, **64**, 1868–1873.
71 H. J. Butt and M. Jaschke, *Nanotechnology*, 1995, **6**, 1.